Mechanism Development for Application of the Theory of Kinestatic Control

Bo Zhang
Carl D. Crane III[1]
Center for Intelligent Machines and Robotics
University of Florida
Gainesville, FL

Michael Griffis
The Eigenpoint Co.
High Springs, FL

Robert Bicker
University of Newcastle-upon-Tyne
Newcastle, UK

Rodney Roberts
Dept. of Electrical and Computer Engineering
Florida State University / Florida A&M University

Abstract

This paper presents the development and testing of a parallel mechanism that is designed to utilize the Theory of Kinestatic Control to simultaneously regulate force/torque and displacement in an application involving a serial robot manipulator. A passive six degree-of-freedom parallel mechanism has been fabricated. This device is designed to be inserted at the end of a serial manipulator, i.e. between the manipulator tool mounting plate and the end effector tooling. The parallel mechanism is instrumented so that the six leg connector lengths are measured and this information together with knowledge of the connector spring constants and free lengths allows for the calculation of the position of the distal end of the mechanism as well as measurement of the currently applied external wrench. The primary contributions of the paper are the development of the forward kinematic position analysis of the special 6-6 geometry of the

[1] Corresponding author: Carl D. Crane III, P.O. Box 116300, Gainesville, FL 32611 ; (352) 219-6433 ; ccrane@ufl.edu.

platform, the development of the theoretical compliance matrix for the fabricated device, and the generation of the experimentally determined compliance matrix which verifies the theoretical development.

Keywords: parallel mechanism, kinematics, compliance, kinestatic control

1. Introduction

Since the mid 1960's, industrial robots have been used more and more to perform various industrial assembly and manipulation tasks. Early applications, such as spray painting and spot welding, could be accomplished by pure position control of the end effector. Rigid body links and stiff actuation would make the robot very stiff which would help in achieving high repeatability in positioning and orienting the end effector.

More complex tasks, however, require control of contact forces in addition to positioning. For example, the simple process of inserting a peg into a hole requires an ability to reposition and reorient the peg based on sensed contact forces. A traditional solution to this problem is to chamfer the edge of the hole, taper the end of the peg, and/or use a Remote Center Compliance (RCC) device, such as shown in Figure 1, between the end effector tool mounting plate and the peg. Here the RCC has high axial stiffness, but low lateral stiffness which when combined with the chamfer applied to the hole, allows for the peg insertion when there is slight position misalignment.

Several theories such as "Hybrid Control" [3] and "Stiffness Control" [2] have been developed to try to solve this problem. Hybrid Control theory relies heavily on the center-of-compliance, which makes it a task-dependent-strategy. Stiffness Control theory allows the location of the center-of-compliance to be selected and adjusts the rotational and translational

compliance properties accordingly. It is essentially calculating a set of variable gains for each joint so the approach becomes task and manipulator dependent. Other researchers such as Huang and Schimmels [10], Roberts [11, 12], Lipkin [13, 14], and Gosselin [15] have researched the spatial stiffness problem.

2. Overview of Kinestatic Control

The theory of Kinestatic Control was proposed by Griffis and Duffy [1] in 1991. In general, the spatial stiffness of a compliant coupling that connects a pair of rigid bodies is used to map a small twist between the bodies into the corresponding interactive wrench. This mapping is based upon a firm geometrical foundation and establishes a positive-definite inner product (elliptic metric) that decomposes a general twist into a twist of freedom and a twist of compliance.

A planar example is shown in Figure 2 [4, 6]. A serial pair of actuated prismatic joints supports a wheel via a two-spring system. The actuated prismatic joints are controlled so that the wheel can maintain a desired contact with a rigid wall. The objective of this simple example is to control the contact force between the wheel and the rigid wall when the wheel is sliding along the surface.

The serial pair of actuated prismatic joints supports the body B_1B_2, which connects with the wheel via two compliant connectors (B_1C and B_2C). The actuator drives the body with pure motion in the *i* and *j* directions to adjust the position of the wheel along the surface and the contact force between the wheel and the surface. Given the compliant proprieties of the two connectors (spring constants and free lengths) and the geometry of the mechanism, the control objective is to determine the displacement changes for the two prismatic actuators, i.e. δd_1 and

δd_2 in order to achieve a desired position of the wheel and contact force between the wheel and the surface. The referenced work [4, 6] presents the solution of this problem together with a numerical example. A significant result of this prior work was that Griffis and Duffy proved that the instantaneous compliance matrix which relates a change in the applied wrench (force for the planar example) to the relative displacement of the compliant mechanism was not symmetric when an external wrench was applied across the compliant mechanism.

For the general spatial case, it is necessary that the compliant mechanism possess six degrees of freedom. One implementation of the device is an in-parallel mechanism where the 'top' platform is connected to the 'base' platform by six S-P-H[2] serial chains which are referred to as the leg connectors (see Figure 3). The term 'in-parallel' is used when the six leg connectors have the same configuration of joint types. In this device, all the joints in the leg connectors are passive, i.e. there are no actuators. The prismatic joint will be compliant, however, and the spring constant and free length of each connector is assumed to be known. Such a device can be inserted between the tool mounting plate of a six degree of freedom industrial manipulator and the end effector tooling as shown in Figure 4. By instrumenting each of the six leg connectors so that the length of each connector can be measured, then the force in each connector and thereby the wrench currently applied to the top platform can be determined. The objective then is to determine how the industrial manipulator should change the position and orientation of the tool mounting plate (attached to the base platform) so that the external wrench that is being experienced at the top platform is as desired. This paper describes the design and initial testing of such a six degree of freedom parallel platform.

[2] An S-P-H chain refers to a series of bodies connected by a spherical joint followed by a prismatic joint followed by a Hooke joint.

3. Platform Design and Analysis

The design process was accomplished in three stages:

- Product specification and planning stage,
- Conceptual design stage,
- Physical design stage.

During the first stage, the functionality, dimension, and other requirements are specified for the development of the device. In the second stage, several rough conceptual design alternatives are developed based on the product specification and the one with the best overall performance is chosen to be developed. In the last stage, the dimensional and functional design, analysis and optimization, assembly simulation, material selection, and engineering documentation are completed.

3.1 Specification and Planning Stage

In the specification and planning stage, the device's geometrical and functional requirements are stated as follows:

- The mechanism should be compliant in nature to measure contact loads,
- The mechanism should have six degrees of freedom,
- The mechanism should be a spatial parallel device,
- The mechanism should be able to measure loads without large errors,
- The device should have a relatively compact size.

Specific design objective specifications are presented in Table 1. Note that the direction of the Z axis is perpendicular to the plane of the base platform

3.2 Conceptual Design Stage

In the conceptual design stage, a 3-3 octahedral structure was first considered (see Figure 3) as this is the simplest six degree of freedom system of its kind. The terminology 3-3 refers to the fact that the device has three connection points on the bottom platform and three connection points on the top platform. The advantage of the 3-3 platform is that the forward position analysis, i.e. the determination of the position and orientation of the top platform with respect to the base platform when given the constant mechanism parameters and the six connector lengths, was shown in [5] to yield a maximum of 16 possible solutions. The approach required the solution of a single 8th degree polynomial in the square of one mechanism variable. The forward position analysis is required so that the pose of the top platform can be determined for use in subsequent force analyses. A simple forward analysis solution will result in a faster solution which will affect the control bandwidth of the device.

Although the 3-3 platform offers the simplest forward analysis solution, the mechanical complexity of the device is high since the device consists of six concentric ball and socket joint pairs. A general 6-6 platform avoids this mechanical design problem; however the forward position analysis of this device would require solution of a 40th order polynomial.

As a result, a new platform design, named the Special 6-6 was conceived. This device is depicted in Figure 5. Here, the concentric ball and socket joints have been separated such that all the base platform connection points lie on a triangle and all the top platform connection points lie on a second triangle. The complexity of the forward analysis of this device is of the same order as that of the 3-3 device. Specifically, a kinematically equivalent 3-3 platform is determined based on the constant mechanism parameters and the six measured leg lengths of the special 6-6 device. The forward position analysis of this kinematically equivalent 3-3 platform is then

performed which yields the position and orientation of the top platform of the Special 6-6 relative to its base platform. Appendix A provides a detailed description of how the equivalent 3-3 platform is obtained from the special 6-6 geometry.

The next issue was to determine the best configuration for the top platform when the device is in its home unloaded configuration. In this analysis, 'best' was defined as the configuration where the Plücker coordinates of the six leg connectors are 'as far as possible' from being linearly dependent. Lee [8] analyzed the 3-3 and Special 6-6 platforms to determine the ratio of the size of the top platform to the base as well as the height and pose of the top platform such that the determinant of the 6×6 matrix formed by the Plücker coordinates of the six leg connectors would be at its maximum value. The result was that if the length of the side of the top platform triangle was a then the optimal unloaded home position pose would occur if the base triangle was twice this size, i.e. $2a$, and the top platform was parallel to the base at a distance a above it while rotated about the Z axis as shown in the configuration in Figure 5.

3.3 Physical Design Stage

The physical design stage first involves identifying specific off-the-shelf hardware components such as the spring and length measurement system for each leg connector and the joint elements to be used at each end of the connectors. Next, custom components must be sized so that the desired performance characteristics identified in Table 1 can be met. Of particular concern is that collisions between the leg connectors be avoided as the top platform moves throughout the desired workspace.

The elastic component is a crucial element for the passive compliant parallel manipulator prototype. Precision linear springs were selected for use as the elastic component to provide

elongation and compression of the leg connectors. After carefully studying and comparing different springs, a group of cylindrical precision springs with different spring constants and the same high linear coefficient (±5%) were selected to use as the elastic component in the legs. The spring rates were respectively 8.755 N/mm, 2.627 N/mm and 0.8755 N/mm (or 50 lb/in, 15lb/in, and 5 lb/in). By using different groups of springs, the stiffness matrix of the parallel platform could be changed by replacing the spring and thus the device can be applied to different applications where the expected force ranges are different.

The free length variation of each connector is measured by a linear optical encoder. Each leg connector is comprised of two parts that translate with respect to each other and are interconnected by the spring. The encoder read head is attached to one of the leg parts and the encoder linear scale is attached to the other. The two leg parts are constrained by a ball spline to ensure that they translate relative to one another and to help maintain alignment of the encoder read head and linear scale.

The requirements for a feasible design were analyzed with regards to dimensional limits for manufacturing parts, encoders available in the market, and the need for a continuous working space with no interference of moving parts. A 3-D model of each leg connector and an assembly simulation were prepared based on this analysis. The critical geometric design parameters are shown in Figure 6 which is a plan view of the conceptual design at the unloaded home position. It was already determined that the length *b* should be twice that of length *a*. From these models, values for the design parameters were chosen to be:

a = 60 mm, b =120 mm,

$\rho_1 = \rho_2 = 28/120 = 0.2333$.

Figure 7 shows the assembled platform device. For the assembled device, the spring constant of each leg was determined experimentally to be 13.65 N/mm and the free lengths of the leg connectors were determined to be 68 mm for three of the connectors and 81 mm for the other three.

4.0 Development of Theoretical and Experimental Compliance Matrix

The compliance matrix is a 6×6 matrix that relates the change in the wrench applied to the top platform to the change in the pose of the top platform. This relationship is written as

$$\delta\hat{w} = [\mathbf{K}]\delta\hat{D} \tag{1}$$

where $\mathbf{K}$ is the compliance matrix, $\delta\hat{w} = [\delta\mathbf{f}; \delta\mathbf{m}]^T$ is the change of the wrench, and $\delta\hat{D} = [\delta\mathbf{X}; \delta\boldsymbol{\varphi}]^T$ is the change in pose. The system testing to be reported here consists of first calculating the theoretical compliance matrix when a wrench is applied to the top platform to displace the top platform from its unloaded home position. This theoretical compliance matrix is then compared to an experimentally determined compliance matrix that is found by applying a wrench to displace the top platform to the same pose considered in the theoretical case. The top platform is then slightly displaced from this pose six times with the change in pose and the change in the applied wrench determined. The experimental compliance matrix can be calculated based on the set of six changes in pose and applied wrench.

4.1 Theoretical Compliance Matrix

It was first shown by Griffis [6] that the compliance matrix for the parallel mechanism may be written as the sum of five matrices as

$$\begin{aligned}[\mathbf{K}] = {} & [\mathbf{j}][k_i][\mathbf{j}]^T + [\delta\mathbf{j}_\theta][k_i(1-\rho_i)][\delta\mathbf{j}_\theta]^T + [\delta\mathbf{j}_\alpha][k_i(1-\rho_i)][\delta\mathbf{j}_\alpha]^T \\ & + [\delta\mathbf{j}_\theta][k_i(1-\rho_i)][V_\theta]^T + [\delta\mathbf{j}_\alpha][k_i(1-\rho_i)][V_\alpha]^T\end{aligned} \tag{2}$$

where **j** is a 6×6 matrix whose columns are the Plücker coordinates of the lines along the six leg connectors and $[k_i]$ is a diagonal 6×6 matrix whose diagonal elements are the spring constants of the six leg connectors. The term ρ_i is defined as

$$\rho_i = \frac{\ell_{0i}}{\ell_i} \tag{3}$$

which is the ratio of the free length of connector *i* to the current length of the connector and the term $[k_i(1-\rho_i)]$ is a diagonal 6×6 matrix whose diagonal elements are given by $k_i(1-\rho_i)$. The terms $[\delta\mathbf{j}_\theta]$ and $[\delta\mathbf{j}_\alpha]$ are each 6×6 matrices whose columns are the derivatives of the Plücker coordinates of the lines along the leg connectors taken with respect to θ_i and α_i which are angles which define the direction of the line along leg *i*. The remaining terms to be defined in equation (2) are $[V_\theta]$ and $[V_\alpha]$. Each column of each of these 6×6 matrices are moments, i.e. the first three elements of each column equal zero. The complete definition of these matrices is presented in [6].

Two coordinate systems must be defined in order to define the relative pose of the top platform relative to the base. Figure 8 shows these coordinate systems which are labeled the *0* and *1* coordinate systems. For the case under consideration, the compliance matrix will be determined when the top platform is moved away from the unloaded position. The pose of the top platform for the case to be analyzed is defined by the following 4×4 transformation matrix:

$$ {}^{0}_{1}\mathbf{T} = \begin{bmatrix} 0.5017 & 0.8647 & -0.0243 & 30.1091 \\ -0.8647 & 0.5021 & 0.0154 & 51.6518 \\ 0.0256 & 0.0133 & 0.9996 & 58.5839 \\ 0 & 0 & 0 & 1 \end{bmatrix} \tag{4}$$

where the units of the terms in the first three columns are dimensionless and the units of the top three terms of the fourth column are millimeters.

The theoretical compliance matrix corresponding to the position of the top platform as defined by ${}^{0}_{1}\mathbf{T}$ was calculated from equation (2) using the geometric and spring values for the fabricated device. The calculated matrix is written as

$$[\mathbf{K}]_{\text{theor}} = \begin{bmatrix} 3.0505 & 0.0426 & -0.0239 & -21.406 & 211.79 & -101.96 \\ 0.0426 & 3.0365 & 0.0265 & -205.78 & -21.241 & 180.95 \\ -0.024 & 0.0265 & 12.101 & 412.15 & -732.38 & 42.647 \\ -21.406 & -210.72 & 411.97 & 33777 & -24895 & -10396 \\ 216.73 & -21.241 & -732.36 & -24898 & 64519 & -11169 \\ -101.78 & 180.93 & 42.647 & -10226 & -10906 & 18475 \end{bmatrix} \tag{5}$$

where the terms of the upper left 3×3 submatrix have units of N/mm, the terms of the upper right and lower left 3×3submatrices have units of N, and where the terms of the lower right 3×3 submatrix have units of N mm.

4.2 Experimental Compliance Matrix

The compliance matrix for the assembled device was determined experimentally for the case where the top platform was positioned and oriented as per (4). The top platform was positioned as per (4) by moving the top platform until the leg lengths, as measured by the optical encoders, were the required length as determined from a reverse position analysis. The applied wrench at this instant was calculated to be

$$\hat{\mathbf{w}}_1 = \begin{bmatrix} 0.0263 \\ 0.1829 \\ -4.9436 \\ -263.1979 \\ 179.5602 \\ 2.7457 \end{bmatrix} \tag{6}$$

where the first three terms have units of Newtons and the last three terms have units of Newton-millimeters.

As previously stated, the stiffness matrix **K** relates the change in the applied wrench to the instantaneous motion of the top platform as per (1). By evaluating the change in the wrench and the twist six times, equation (1) can be written in matrix format as

$$[\delta\hat{\mathbf{w}}_{6\times6}] = [\mathbf{K}][\delta\hat{\mathbf{D}}_{6\times6}] \tag{7}$$

where $[\delta\hat{\mathbf{w}}_{6\times6}]$ and $[\delta\hat{\mathbf{D}}_{6\times6}]$ are 6×6 matrices defined as

$$[\delta\hat{\mathbf{w}}_{6\times6}] = \begin{bmatrix}\delta\hat{\mathbf{w}}_{1\to A} & \delta\hat{\mathbf{w}}_{1\to B} & \delta\hat{\mathbf{w}}_{1\to C} & \delta\hat{\mathbf{w}}_{1\to D} & \delta\hat{\mathbf{w}}_{1\to E} & \delta\hat{\mathbf{w}}_{1\to F}\end{bmatrix} \tag{8}$$

$$[\delta\hat{\mathbf{D}}_{6\times6}] = \begin{bmatrix}\delta\hat{\mathbf{D}}_{1\to A} & \delta\hat{\mathbf{D}}_{1\to B} & \delta\hat{\mathbf{D}}_{1\to C} & \delta\hat{\mathbf{D}}_{1\to D} & \delta\hat{\mathbf{D}}_{1\to E} & \delta\hat{\mathbf{D}}_{1\to F}\end{bmatrix}. \tag{9}$$

The columns of $[\delta\hat{\mathbf{w}}_{6\times6}]$ are the changes in the external wrench as the platform moved from position 1 to position A, position 1 to position B, etc. The columns of $[\delta\hat{\mathbf{D}}_{6\times6}]$ are the twists that represent the motion of the platform from position 1 to position A, from position 1 to position B, etc. Once the matrices $[\delta\hat{\mathbf{w}}_{6\times6}]$ and $[\delta\hat{\mathbf{D}}_{6\times6}]$ are determined, the stiffness matrix can be calculated as

$$[\mathbf{K}]_{\text{exp}} = [\delta\hat{\mathbf{w}}_{6\times6}][\delta\hat{\mathbf{D}}_{6\times6}]^{-1}\ . \tag{10}$$

The top platform was moved to six poses that were close to the previous pose. These poses are named A through F. The leg lengths at each pose were measured and the pose of the top platform and the applied wrench were calculated as

$${}^{0}_{A}\mathbf{T} = \begin{bmatrix} 0.5391 & 0.8420 & -0.0191 & 30.8315 \\ -0.8419 & 0.5394 & 0.0164 & 51.0055 \\ 0.0241 & 0.0072 & 0.9997 & 58.5788 \\ 0 & 0 & 0 & 1 \end{bmatrix}, \quad \hat{\mathbf{w}}_{A} = \begin{bmatrix} 4.7730 \\ 2.2219 \\ -4.8295 \\ -433.9854 \\ 508.2140 \\ 138.8671 \end{bmatrix},$$

$$
{}^{0}_{B}\mathbf{T}=\begin{bmatrix} 0.5041 & 0.8633 & -0.0237 & 30.0674 \\ -0.8637 & 0.5040 & -0.0068 & 51.5888 \\ 0.0061 & 0.0239 & 0.9997 & 58.6874 \\ 0 & 0 & 0 & 1 \end{bmatrix},\ \hat{\mathbf{w}}_{B}=\begin{bmatrix} -0.3449 \\ -0.4166 \\ -8.4476 \\ -223.6900 \\ 363.1519 \\ -21.4402 \end{bmatrix},
$$

$$
{}^{0}_{C}\mathbf{T}=\begin{bmatrix} 0.5019 & 0.8648 & -0.0099 & 30.0147 \\ -0.8645 & 0.5020 & 0.0242 & 51.4415 \\ 0.0259 & -0.0036 & 0.9997 & 58.6024 \\ 0 & 0 & 0 & 1 \end{bmatrix},\quad \hat{\mathbf{w}}_{C}=\begin{bmatrix} 0.3539 \\ -0.5456 \\ -8.1272 \\ -370.3918 \\ 465.1178 \\ -63.1008 \end{bmatrix},
$$

$$
{}^{0}_{D}\mathbf{T}=\begin{bmatrix} 0.4778 & 0.8781 & -0.0265 & 30.4274 \\ -0.8782 & 0.4782 & 0.0109 & 52.4777 \\ 0.0222 & 0.0181 & 0.9996 & 58.6251 \\ 0 & 0 & 0 & 1 \end{bmatrix},\hat{\mathbf{w}}_{D}=\begin{bmatrix} -0.6523 \\ 0.1190 \\ -5.7095 \\ -257.3332 \\ 156.5356 \\ -88.9454 \end{bmatrix},
$$

$$
{}^{0}_{E}\mathbf{T}=\begin{bmatrix} 0.5097 & 0.8602 & -0.0165 & 31.7774 \\ -0.8601 & 0.5099 & 0.0154 & 52.0331 \\ 0.0217 & 0.0064 & 0.9997 & 58.7887 \\ 0 & 0 & 0 & 1 \end{bmatrix},\quad \hat{\mathbf{w}}_{E}=\begin{bmatrix} 5.8796 \\ 2.0262 \\ -4.8078 \\ -420.4532 \\ 600.3909 \\ -47.7374 \end{bmatrix},
$$

$$
{}^{0}_{F}\mathbf{T}=\begin{bmatrix} 0.4993 & 0.8659 & -0.0305 & 30.4078 \\ -0.8661 & 0.4998 & 0.0084 & 50.0301 \\ 0.0225 & 0.0222 & 0.9995 & 58.5063 \\ 0 & 0 & 0 & 1 \end{bmatrix},\hat{\mathbf{w}}_{F}=\begin{bmatrix} 0.3890 \\ -4.9762 \\ -5.0937 \\ 125.7469 \\ 212.4282 \\ -329.0032 \end{bmatrix}. \qquad (11)
$$

The matrix $[\delta\hat{\mathbf{w}}_{6\times6}]$ is relatively simple to calculate. The change in the wrench, $\delta\hat{\mathbf{w}}_{1\to A}$ is simply calculated as the difference between these two wrenches as

$$\delta\hat{\mathbf{w}}_{1\to A} = \hat{\mathbf{w}}_A - \hat{\mathbf{w}}_1 \quad . \tag{12}$$

Similar calculations are performed for the other five legs. The matrix $[\delta\hat{\mathbf{w}}_{6\times6}]$ was calculated as

$$[\delta\hat{\mathbf{w}}_{6\times6}] = \begin{bmatrix} 4.7467 & -0.3712 & 0.3277 & -0.6785 & 5.8533 & 0.3628 \\ 2.0391 & -0.5994 & -0.7285 & -0.0639 & 1.8434 & -5.1591 \\ 0.1141 & -3.5041 & -3.1836 & -0.7659 & 0.1358 & -0.1501 \\ -170.79 & 39.508 & -107.19 & 5.8646 & -157.26 & 388.94 \\ 337.65 & 192.59 & 294.56 & -14.025 & 429.82 & 41.868 \\ 136.12 & -24.186 & -65.847 & -91.691 & -50.483 & -331.75 \end{bmatrix} \tag{13}$$

where the terms in the first three rows have units of N and those of the last three rows have units of N mm.

The determination of the twists as the top platform moves from position 1 to each of the six other positions is slightly more complicated. The determination of the twist $\delta\hat{\mathbf{D}}_{1\to A}$ will be presented.

The twist $\delta\hat{\mathbf{D}}_{1\to A}$ is comprised of six components. When written in axis coordinates, the last three represent the instantaneous angular velocity of the moving body and the first three represent the instantaneous linear velocity of a point in the moving body that is coincident with the origin of the reference frame. In this case, both of these instantaneous quantities must be approximated from the finite motion of the platform as it moves between pose 1 and pose A.

The angular velocity was approximated by calculating the axis and angle of rotation that would rotate the top coordinate system from its orientation at pose 1 to its orientation at pose A. This was accomplished by first evaluating the net rotation matrix that relates the A pose to the 1 pose as

$$ {}^{1}_{A}\mathbf{R} = \left[{}^{0}_{1}\mathbf{R} \right]^{T} \; {}^{0}_{A}\mathbf{R} \tag{14} $$

where the 3×3 rotation matrices ${}^{0}_{1}\mathbf{R}$ and ${}^{0}_{A}\mathbf{R}$ are obtained as the upper left 3×3 elements of the transformation matrices ${}^{0}_{1}\mathbf{T}$ and ${}^{0}_{A}\mathbf{T}$ respectively. For this case the rotation matrix ${}^{1}_{A}\mathbf{R}$ was evaluated as

$$ {}^{1}_{A}\mathbf{R} = \begin{bmatrix} 0.999 & -0.0438 & 0.0018 \\ 0.0437 & 0.999 & 0.0050 \\ -0.0020 & -0.0049 & 1.0000 \end{bmatrix}. \tag{15} $$

The angle of rotation and axis of rotation that would rotate coordinate system 1 to be aligned with coordinate system A are calculated as θ=2.526 degrees and ${}^{0}\mathbf{m}$ = [-0.0433, 0.1342, 0.9900]^{T}. The superscript associated with the axis vector **m** is used to indicate that the rotation axis that was determined from (15) was expressed in terms of the coordinate system attached to the base platform. Finally, the last three components of $\hat{\mathbf{D}}_{1\to A}$ are approximated by (θ ${}^{0}\mathbf{m}$) and will be dimensionless (radians).

As previously stated, the first three components of $\hat{\mathbf{D}}_{1\to A}$ represent the instantaneous linear velocity of a point in the moving body that is coincident with the origin of the reference frame. This quantity is estimated by first determining the coordinates of the origin point of the ground, 0, coordinate system in the 1 coordinate system, i.e., ${}^{1}\mathbf{P}_{0\text{orig}}$. This quantity is determined as

$$ {}^{1}\mathbf{P}_{0\text{orig}} = -\left[{}^{0}_{1}\mathbf{R} \right]^{T} \; {}^{0}\mathbf{P}_{1\text{orig}} \tag{16} $$

where ${}^{0}\mathbf{P}_{1\text{orig}}$ is obtained as the top three terms of the fourth column of ${}^{0}_{1}\mathbf{T}$ which was numerically determined in (4). For infinitesimal motion, the coordinates of the origin of the ground coordinate system should be the same when measured in the 1 or the A coordinate

systems. Thus it is assumed that ${}^{A}\mathbf{P}_{0'\text{orig}} = {}^{1}\mathbf{P}_{0\text{orig}}$ where the notation *0'orig* is introduced. This point is then transformed to the 1 coordinate system as

$$ {}^{1}\mathbf{P}_{0'\text{orig}} = {}^{1}_{A}\mathbf{T}\ {}^{A}\mathbf{P}_{0'\text{orig}} \tag{17} $$

where

$$ {}^{1}_{A}\mathbf{T} = \left[{}^{0}_{1}\mathbf{T}\right]^{-1}\ {}^{0}_{A}\mathbf{T}\ . \tag{18} $$

The translation of the origin point of coordinate system 0 as seen from coordinate system 1 can be written as the net displacement of the point as

$$ {}^{1}\mathbf{v}_{0\text{orig}} = {}^{1}\mathbf{P}_{0'\text{orig}} - {}^{1}\mathbf{P}_{0\text{orig}}\ . \tag{19} $$

Lastly, this translation vector can be evaluated in the 0 coordinate system as

$$ {}^{0}\mathbf{v}_{o} = {}^{0}_{1}\mathbf{R}\ {}^{1}\mathbf{v}_{0\text{orig}}\ . \tag{20} $$

For this particular case, the translation of the point in the top platform that is coincident with the origin of the reference coordinate system, for the case where the top platform moves from pose 1 to pose A, was evaluated as

$$ {}^{0}\mathbf{v}_{o} = \begin{bmatrix} 2.6613 \\ -2.0298 \\ -0.2672 \end{bmatrix} \text{mm}\ . \tag{21} $$

Thus for the case where the top platform moves from position 1 to position A, the instantaneous twist written in axis coordinates is estimated as

$$ \hat{\mathbf{D}}_{1\to A} = \begin{bmatrix} {}^{0}\mathbf{v}_{o} \\ \theta\ {}^{0}\mathbf{m} \end{bmatrix} = \begin{bmatrix} 2.6613 \\ -2.0298 \\ -0.2672 \\ -0.00191 \\ 0.00592 \\ 0.04364 \end{bmatrix} \tag{22} $$

where the first three components have units of mm and the last three components have units of rad.

The process can be repeated to determine the twists associated with the motion from pose 1 to pose B, pose 1 to pose C, …, pose 1 to pose F. The resulting twists were determined as

$$\hat{\mathbf{D}}_{1\to B}=\begin{bmatrix}-0.0625\\1.1674\\-1.0111\\0.0222\\0.0006\\0.0027\end{bmatrix},\quad \hat{\mathbf{D}}_{1\to C}=\begin{bmatrix}-0.9372\\-0.7173\\0.9138\\-0.0088\\0.0144\\-0.0001\end{bmatrix},\quad \hat{\mathbf{D}}_{1\to D}=\begin{bmatrix}-0.9282\\1.9750\\-0.3058\\0.0053\\-0.0025\\-0.0273\end{bmatrix},$$

$$\hat{\mathbf{D}}_{1\to E}=\begin{bmatrix}1.6751\\0.1013\\0.4494\\-0.0001\\0.0079\\0.0091\end{bmatrix},\quad \hat{\mathbf{D}}_{1\to F}=\begin{bmatrix}0.5338\\-1.1276\\-0.6290\\0.0071\\-0.0062\\-0.0025\end{bmatrix}. \tag{23}$$

Lastly, substituting these values into (9) and then substituting (9) and (13) into (10) yields the stiffness matrix for the device at pose 1. This matrix was determined as

$$[\mathbf{K}]_{\text{exp}}=\begin{bmatrix}2.9045 & -0.0499 & 1.7812 & 67.167 & 136.53 & -97.152\\-0.0239 & 2.9637 & 0.8046 & -167.05 & -56.028 & 181.38\\0.2085 & 0.0308 & 11.182 & 364.17 & -693.53 & 32.81\\-8.5556 & -205.44 & 326.45 & 29390 & -21122 & -10796\\189.53 & -29.633 & -524.65 & -14459 & 55733 & -10174\\-98.136 & 179.71 & 18.616 & -11395 & -9997.3 & 18204\end{bmatrix} \tag{24}$$

where the units of the elements of (24) are the same as those of (5).

4.3 Comparison of Theoretical and Experimental Compliance Matrices

Comparing the experimentally determined compliance matrix (24) with the theoretical compliance matrix (5), it is apparent that they are close and consistent. To better perform the comparison, the case of six linearly independent twists will be considered and the corresponding changes in the externally applied wrench will be calculated using the theoretical and experimental compliance matrices. These changes in the applied wrench can then be compared.

The six twists are selected to be the three rotations about the axes of the coordinate system attached to the top platform and the three translations along these axes. These twists are calculated in terms of the coordinate system attached to the base platform as

$$\delta\hat{\mathbf{D}}_1 = \begin{bmatrix} 51.9798 \\ 28.6207 \\ -51.9490 \\ 0.5017 \\ -0.8647 \\ 0.0256 \end{bmatrix}, \quad \delta\hat{\mathbf{D}}_2 = \begin{bmatrix} -28.7280 \\ 50.2570 \\ -29.5455 \\ 0.8647 \\ 0.5021 \\ 0.0133 \end{bmatrix}, \quad \delta\hat{\mathbf{D}}_3 = \begin{bmatrix} 50.7289 \\ -31.5206 \\ 1.7188 \\ -0.0243 \\ 0.0154 \\ 0.9996 \end{bmatrix},$$
$$\delta\hat{\mathbf{D}}_4 = \begin{bmatrix} 0.5017 \\ -0.8647 \\ 0.0256 \\ 0 \\ 0 \\ 0 \end{bmatrix}, \quad \delta\hat{\mathbf{D}}_5 = \begin{bmatrix} 0.8647 \\ 0.5021 \\ 0.0133 \\ 0 \\ 0 \\ 0 \end{bmatrix}, \quad \delta\hat{\mathbf{D}}_6 = \begin{bmatrix} -0.0243 \\ 0.0154 \\ 0.9996 \\ 0 \\ 0 \\ 0 \end{bmatrix} \tag{25}$$

where the first three terms have units of mm and the last three are dimensionless. Note that the direction of the line of action for all three rotations has been unitized and the direction for all three translations has also been unitized.

The six changes to the applied wrench as determined by use of the theoretical compliance matrix in (5) are written as columns of the following matrix:

$$\delta\hat{\mathbf{w}}_{\text{th}} = \begin{bmatrix} -35.4592 & 1.6862 & 55.2273 & 1.4930 & 2.6588 & -0.0974 \\ 7.5042 & -35.5977 & 92.0451 & -2.6036 & 1.5618 & 0.0722 \\ 212.032 & -366.284 & 40.0827 & 0.2748 & 0.1535 & 12.0972 \\ 9661.40 & -5578.16 & -5331.78 & 182.017 & -118.833 & 409.080 \\ -19863.8 & 25061.4 & 839.302 & 108.352 & 167.001 & -737.661 \\ 2445.37 & -3315.69 & 7755.23 & -206.421 & 3.4030 & 47.890 \end{bmatrix}. \quad (26)$$

The six changes to the applied wrench as determined by use of the experimentally determined compliance matrix in (24) are written as columns of the following matrix:

$$\delta\hat{\mathbf{w}}_{\text{ex}} = \begin{bmatrix} -29.8314 & -13.2359 & 55.3339 & 1.5459 & 2.5102 & 1.7091 \\ 11.0646 & -44.3063 & 91.2567 & -2.5541 & 1.4781 & 0.8505 \\ 214.0645 & -367.71 & 42.0932 & 0.3642 & 0.3448 & 11.1729 \\ 9449.45 & -5059.57 & -5228.44 & 181.709 & -106.208 & 323.364 \\ -19448.2 & 23912.5 & 686.642 & 107.280 & 142.030 & -529.502 \\ 2469.08 & -3329.86 & 7708.74 & -204.153 & 5.6218 & 23.7608 \end{bmatrix}. \quad (27)$$

In both (26) and (27), the terms in the top three rows have units of N and the terms in the bottom three rows have units of N mm.

Several comparisons can be made between the wrenches determined from the theoretical and experimental compliance matrices. The factors to be compared here are the difference between the magnitudes and pitches of the two wrenches as well as the angular difference of the directions of the lines of action along the wrenches and the perpendicular distance between these lines of action. Tables 2 through 4 show the calculated results for the six pairs of wrenches that are being compared.

From the data presented in the Tables it can be seen that there is good agreement between the theoretically determined and experimentally determined change in wrench. The magnitudes of wrenches are quite close although in case 2 there is a difference of 2.6 N. The percent difference for this case is only 0.70%. The magnitude of the rotational twist was quite large

which caused the corresponding calculated wrenches to have large magnitudes, but these calculated magnitudes are relatively very close.

Similarly the difference between the pitches of the theoretically calculated and experimentally calculated wrenches are on the whole quite close, with the largest difference occurring in case 2. Here the percent difference does appear significant.

Ideally, all valued in Table 4 would be zero. The lines of action of all the theoretically determined and experimentally determined changes in wrench lie within an average of 0.48 mm of each other. The directions of the lines of action are almost parallel, although the largest error occurs when the top platform is translated parallel to the Z axis of the coordinate system attached to the top platform.

In summary, although it is very difficult to compare all the parameters associated with the two compliance matrices (equations (5) and (24)), there is good agreement between the theoretically determined and experimentally determined change in wrench associated with the six twists considered here. A more thorough statistical analysis could identify a reliable error range for the change in wrench associated with any arbitrary twist throughout the entire workspace of the mechanism.

5. Conclusion

This paper has presented the design, fabrication, and initial testing of a compliant parallel platform that is to be used in the future as a wrist on industrial manipulators for force control applications. It has been shown how knowledge of the measured leg connector lengths combined with the spring parameters and mechanism geometry parameters results in a compliant system whose compliance matrix as determined experimentally matches the theoretically

determined matrix. This work will allow for an implementation of the Theory of Kinestatic Control where a spatial manipulator can be commanded to move the base platform in order to change the wrench experienced at the top platform.

6. Acknowledgements

The authors would like to acknowledge the immense contributions of Dr. Joseph Duffy who introduced several of the authors to world of spatial mechanisms. His guidance, mentorship, and friendship will not be forgotten. The authors would also like to gratefully acknowledge the support provided by the Department of Energy via the University Research Program in Robotics (URPR), grant number DE-FG04-86NE37967.

7. References

1. M. Griffis, J. Duffy, Kinestatic Control: A Novel Theory for Simultaneously Regulating Force and Displacement, Transactions of the ASME, 508/ Vol. 113, Dec. 1991.
2. Salisbury, J.K., 1980, "Active Stiffness Control of a Manipulator in Cartesian Coordinates", Proceedings of the 19th IEEE Decision and control Conference, Albuquerque, NM
3. Raibert, M., and Craig, J., 1981, "Hybrid Position/ Force Control of Manipulators", ASME Journal of Dynamic Systems, Measurement and Control, Vol. 102
4. Joseph Duffy, "Statics and Kinematics with applications to robotics", Cambridge University press, USA, 1996
5. Griffis, M., and Duffy, J., 1989, "A Forward Displacement Analysis of a Class of Stewart Platforms," Journal of Robotic Systems, John Wiley.
6. Griffis, M. "Kinestatic control: A novel theory for simultaneously regulating force and displacement", Ph.D. Dissertation, University of Florida, Gainesville, FL, 1991.
7. Lee, J., Duffy, J., and Hunt K., "A Practical Quality Index Based On The Octahedral Manipulator," International Journal of Robotic Research, Vol.17, no.10,1081-1090, 1998.

8. Lee, J., “Investigation of quality indices of in-parallel platform manipulators and development of web based analysis tool”, Ph.D Dissertation, University of Florida, Gainesville, FL, 2000
9. Griffis, M., and Duffy, J., “Method and apparatus for controlling geometrically simple parallel mechanisms with distinctive connections,” U.S. Patent number 5,179,525, 12 January 1993
10. Huang, S. and Schimmels, J., “The eigenscrew decomposition of spatial stiffness matrices”, IEEE Tran. on robotics and automation Vol.6 No.2. pp.146-156, 2000.
11. Roberts, R.G., “On the normal form of a spatial stiffness matrix”, Proc. 2002 IEEE Int. Conf. On Robotics and Automation (ICRA) Washington, D.C., pp. 556-561, 2002
12. Roberts, R.G., “Minimal Realization of an Arbitrary Spatial Stiffness Matrix with a Parallel Connection of Simple and Complex Springs”, IEEE Tran. on Robotics and Automation, Vol. 16, NO. 5, pp. 603-608, 2000
13. Ciblak, N., and Lipkin, H., “Synthesis of Cartesian Stiffness for Robotic Applications,” Proceedings of the IEEE International Conference on Robotics, 1999.
14. Lipkin, H., and Patterson, T., “Generalized Center of Compliance and Stiffness,” Proceedings of the IEEE International Conference on Robotics and Automation, 1992.
15. Gosselin, C. 1990. Stiffness mapping for parallel manipulators . IEEE Transactions on Robotics and Automation 6(3): 377-383

Appendix A – Conversion of Special 6-6 Platform to Equivalent 3-3 Platform

A Special 6-6 platform is defined as one which is geometrically reducible to an equivalent 3-3 platform. Figure A1 depicts a perspective and plan view of a 6-6 platform where the leg connector points R_0, S_0, and T_0 lie along the edges of the triangle defined by points O_0, P_0, and Q_0 and the leg connector points O_1, P_1, and Q_1 lie along the edges of the triangle defined by the points R_1, S_1, and T_1. The objective here is to determine the distance between the pairs of points O_0 - R_1, O_0 - S_1, P_0 - S_1, P_0 -T_1 , Q_0 - T_1, and Q_0 - R_1. These distances represent the leg connector lengths for an equivalent 3-3 platform.

Throughout this analysis, the notation m_in_j will be used to represent the distance between the two points M_i and N_j and the notation $\mathbf{m_in_j}$ will represent the vector from point M_i to N_j. Using this notation, the problem statement can be written as:

given: o_0o_1, p_0p_1, q_0q_1, r_0r_1, s_0s_1, t_0t_1 *leg connector lengths for Special 6-6 platform*

o_0p_0, p_0q_0, q_0o_0, o_0s_0, p_0t_0, q_0r_0 *base triangle parameters*

r_1s_1, s_1t_1, t_1r_1, r_1o_1, s_1p_1, t_1q_1 *top triangle parameters*

find: o_0r_1, o_0s_1, p_0s_1, p_0t_1, q_0t_1, q_0r_1 *leg connector lengths for equivalent 3-3 platform*

Obviously it is the case that

$$s_0p_0 = o_0p_0 - o_0s_0 \;\; ; \quad t_0q_0 = p_0q_0 - p_0t_0 \;\; ; \quad r_0o_0 = q_0o_0 - q_0r_0$$

$$o_1s_1 = r_1s_1 - r_1o_1 \;\; ; \quad p_1t_1 = s_1t_1 - s_1p_1 \;\; ; \quad q_1r_1 = t_1r_1 - t_1q_1 \; . \tag{A-1}$$

The six leg connectors of the equivalent 3-3 platform define an octahedron, i.e. there are eight triangular faces; the top and bottom platform triangles and six faces defined by two intersecting connectors and an edge of either the base or top platform. The solution begins by first defining angles β and γ which, for each of the six faces defined by intersecting connectors, defines the angle in the plane between a connector of the Special 6-6 platform and an edge of

either the top or base platform as appropriate. Figure A-2 shows the angles γ_1 and β_1. The angle γ_2 is defined as the angle between $\mathbf{r_0r_1}$ and $\mathbf{r_0o_0}$ and the angle γ_3 is defined as the angle between $\mathbf{s_0s_1}$ and $\mathbf{s_0o_0}$. Similarly, the angle β_2 is defined as the angle between $\mathbf{q_1t_1}$ and $\mathbf{q_1q_0}$ and the angle β_3 is defined as the angle between $\mathbf{o_1s_1}$ and $\mathbf{o_1o_0}$.

Figure A-3 shows a planar triangle that is defined by the vertex points G_1, G_2, and G_3. A point G_0 is defined as a point on the line defined by G_1 and G_2 and the angle φ is shown as the angle between $\mathbf{g_0g_2}$ and $\mathbf{g_0g_3}$. The cosine law for the triangle defined by points G_0, G_2, and G_3 yields

$$\cos\varphi = \frac{b^2 + c^2 - \ell_b{}^2}{2\,b\,c} \quad . \tag{A-2}$$

Next consider that the triangle lies in a plane defined by u and v coordinate axes. The coordinates of any point G_i may then be written as (u_i, v_i). The distance ℓ_a may then be expressed as

$$\begin{aligned} \ell_a{}^2 &= (u_3 - u_1)^2 + (v_3 - v_1)^2 \\ &= (a + c\cos\varphi)^2 + (c\sin\varphi)^2 \\ &= c^2(\sin^2\varphi + \cos^2\varphi) + a^2 + 2\,a\,c\cos\varphi \\ &= a^2 + c^2 + 2\,a\,c\cos\varphi \end{aligned} \quad . \tag{A-3}$$

Substituting (A-2) into (A-3) and simplifying gives

$$\begin{aligned} \ell_a{}^2 &= a^2 + c^2 + \frac{a}{b}(b^2 + c^2 - \ell_b{}^2) \\ &= \frac{1}{b}(b\,a^2 + b\,c^2 + a\,b^2 + a\,c^2 - a\,\ell_b{}^2) \end{aligned} \quad . \tag{A-4}$$

Regrouping this equation gives

$$b\,\ell_a{}^2 + a\,\ell_b{}^2 = (a+b)\,c^2 + a\,b^2 + a^2\,b \quad . \tag{A-5}$$

The result of equation (A-5) can be applied to each of the six side faces of the octahedron defined by the leg connectors of the equivalent 3-3 platform. The parameter substitutions are shown in Table A-1.

Table A-1: Parameter Substitutions

φ	G_0	G_1	G_2	G_3	a	b	c	ℓ_a	ℓ_b
β_1	P_1	T_1	S_1	P_0	p_1t_1	p_1s_1	p_0p_1	p_0t_1	p_0s_1
β_2	Q_1	R_1	T_1	Q_0	q_1r_1	t_1q_1	q_0q_1	q_0r_1	q_0t_1
β_3	O_1	S_1	R_1	O_0	s_1o_1	o_1r_1	o_0o_1	o_0s_1	o_0r_1
γ_1	T_0	P_0	Q_0	T_1	p_0t_0	t_0q_0	t_0t_1	p_0t_1	q_0t_1
γ_2	R_0	Q_0	O_0	R_1	q_0r_0	r_0o_0	r_0r_1	q_0r_1	o_0r_1
γ_3	S_0	O_0	P_0	S_1	o_0s_0	s_0p_0	s_0s_1	o_0s_1	p_0s_1

Using Table A-1 to perform appropriate parameter substitutions in (A-5) will result in six equations that can be written in matrix form as

$$\mathbf{A}\,\mathbf{q} = \mathbf{m} \tag{A-6}$$

where

$$\mathbf{A} = \begin{bmatrix} p_1s_1 & p_1t_1 & 0 & 0 & 0 & 0 \\ 0 & 0 & t_1q_1 & q_1r_1 & 0 & 0 \\ 0 & 0 & 0 & 0 & o_1r_1 & s_1o_1 \\ t_0q_0 & 0 & 0 & p_0t_0 & 0 & 0 \\ 0 & 0 & r_0o_0 & 0 & 0 & q_0r_0 \\ 0 & o_0s_0 & 0 & 0 & s_0p_0 & 0 \end{bmatrix} \quad \mathbf{q} = \begin{bmatrix} p_0t_1^{\,2} \\ p_0s_1^{\,2} \\ q_0r_1^{\,2} \\ q_0t_1^{\,2} \\ o_0s_1^{\,2} \\ o_0r_1^{\,2} \end{bmatrix} \quad \mathbf{M} = \begin{bmatrix} M_1 \\ M_2 \\ M_3 \\ M_4 \\ M_5 \\ M_6 \end{bmatrix} \tag{A-7}$$

and where

$$M_1 = (p_1t_1+p_1s_1)\, p_0p_1^{\,2} + p_1t_1\, p_1s_1^{\,2} + p_1t_1^{\,2}\, p_1s_1 \,,$$

$$M_2 = (q_1r_1+t_1q_1)\, q_0q_1^{\,2} + q_1r_1\, t_1q_1^{\,2} + q_1r_1^{\,2}\, t_1q_1 \,,$$

$$M_3 = (s_1o_1+o_1r_1)\, o_0o_1^{\,2} + s_1o_1\, o_1r_1^{\,2} + s_1o_1^{\,2}\, o_1r_1 \,,$$

$$M_4 = (p_0t_0+t_0q_0)\, t_0t_1^{\,2} + p_0t_0\, t_0q_0^{\,2} + p_0t_0^{\,2}\, t_0q_0 \,,$$

$$M_5 = (q_0r_0+r_0o_0)\, r_0r_1^{\,2} + q_0r_0\, r_0o_0^{\,2} + q_0r_0^{\,2}\, r_0o_0 \,,$$

$$M_6 = (o_0s_0+s_0p_0)\, s_0s_1^{\,2} + o_0s_0\, s_0p_0^{\,2} + o_0s_0^{\,2}\, s_0p_0 \,. \qquad \text{(A-8)}$$

All the terms in matrix **A** are known as they are expressed in terms of given distances of the top and bottom platform. All the terms in vector **m** are known as they are expressed in terms of given dimensions as well as the square of the lengths of the six leg connectors of the Special 6-6 platform. Thus the square of the lengths of the connectors for the equivalent 3-3 platform may be determined as

$$\mathbf{q} = \mathbf{A}^{-1}\, \mathbf{m} \,. \qquad \text{(A-9)}$$

It is interesting to note that the matrix **A** is singular if and only if the following condition is satisfied:

$$\frac{s_0p_0}{s_1p_1}\,\frac{t_0q_0}{t_1q_1}\,\frac{o_0r_0}{o_1r_1} = \frac{q_0r_0}{q_1r_1}\,\frac{o_0s_0}{o_1s_1}\,\frac{p_0t_0}{p_1t_1} \,. \qquad \text{(A-10)}$$

One case where this would occur would be if the location of the connection points S_0, T_0, R_0, O_1, P_1, and Q_1 were all located at the midpoint of the edge on which they lie.

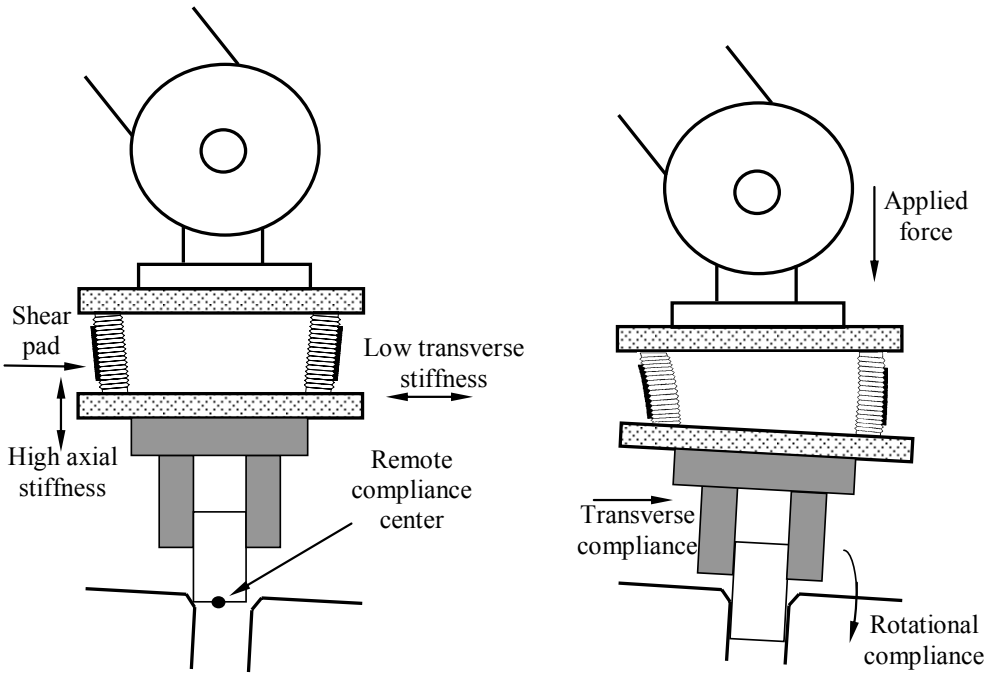

Figure 1: Typical Remote Center Compliance Device (RCC)

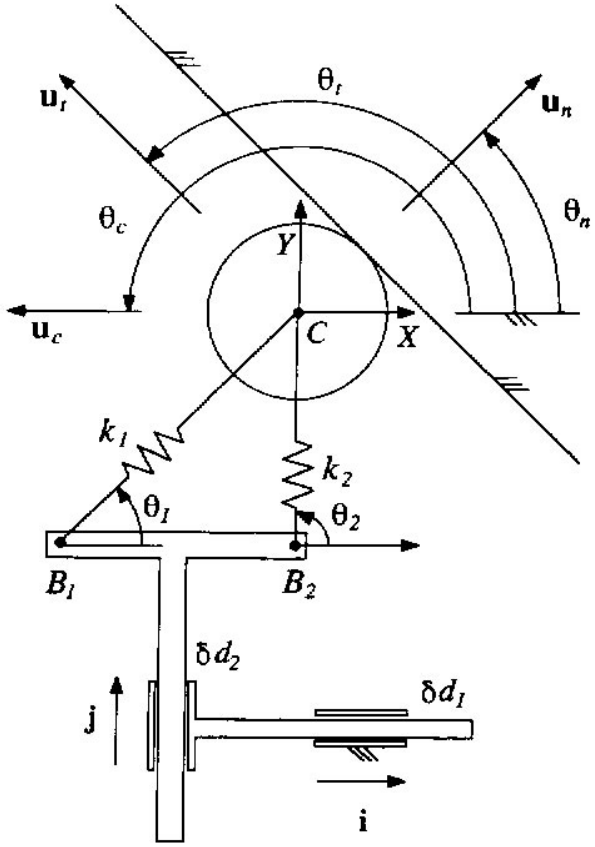

Figure 2: Passive Compliance Device for Contact Force Control

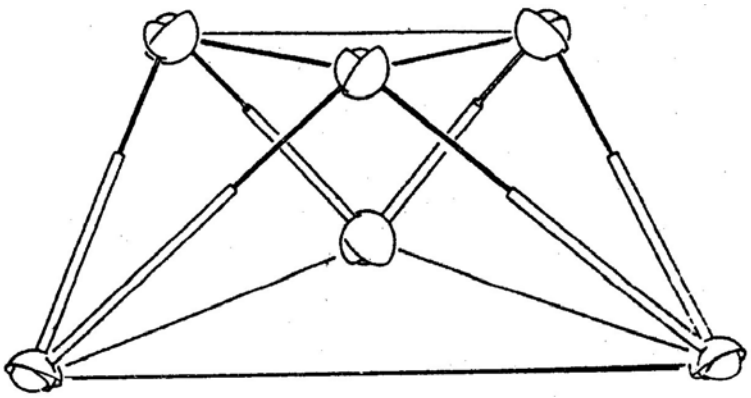

Figure 3: Passive In-Parallel Platform.

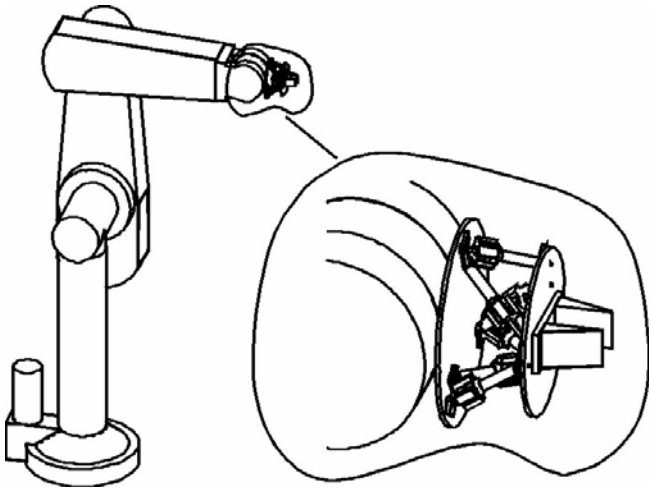

Figure 4: Compliant Platform Inserted between Tool Mounting Plate and End Effector

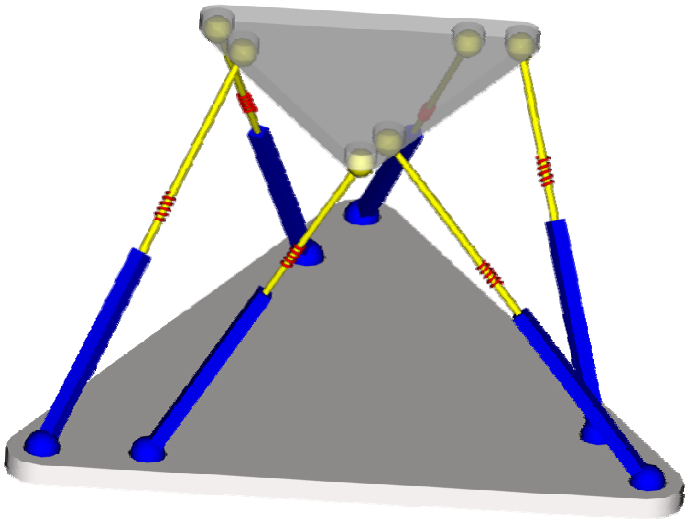

Figure 5: Special 6-6 Platform

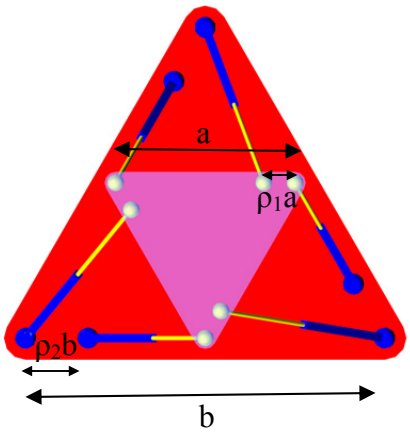

Figure 6. Plan View of Special 6-6 Platform

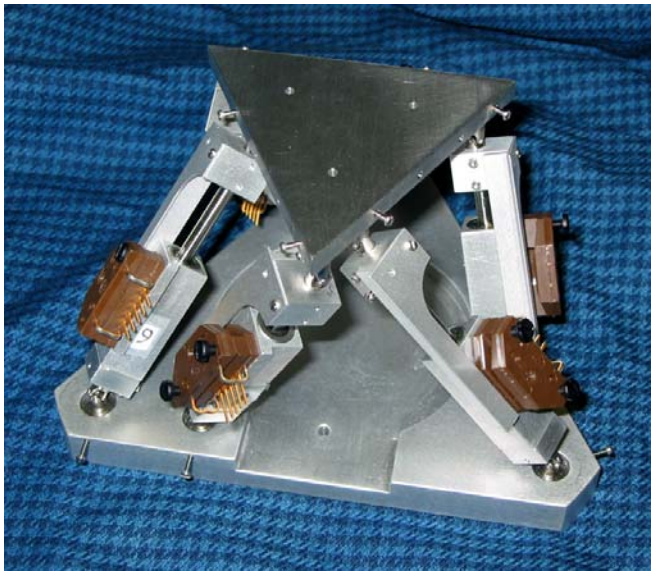

Figure 7: Assembled Compliant Platform

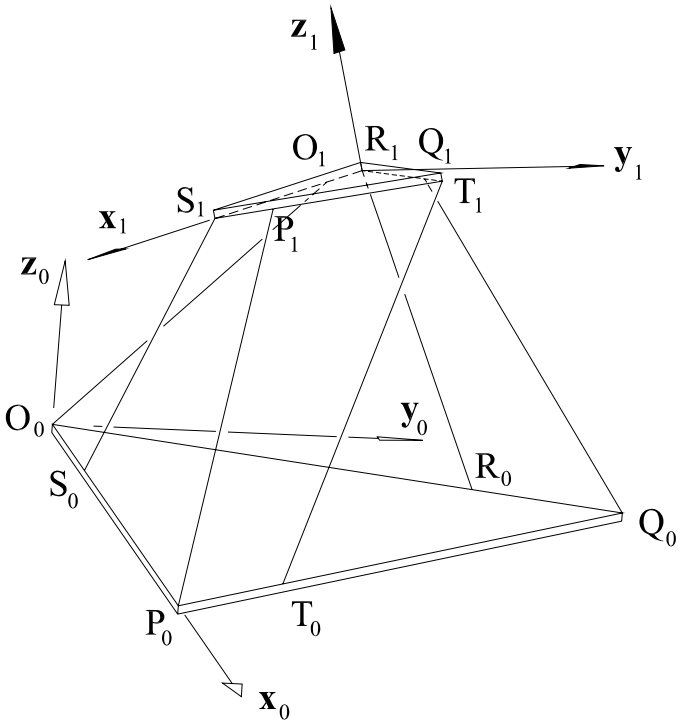

Figure 8: Definition of Coordinate Systems

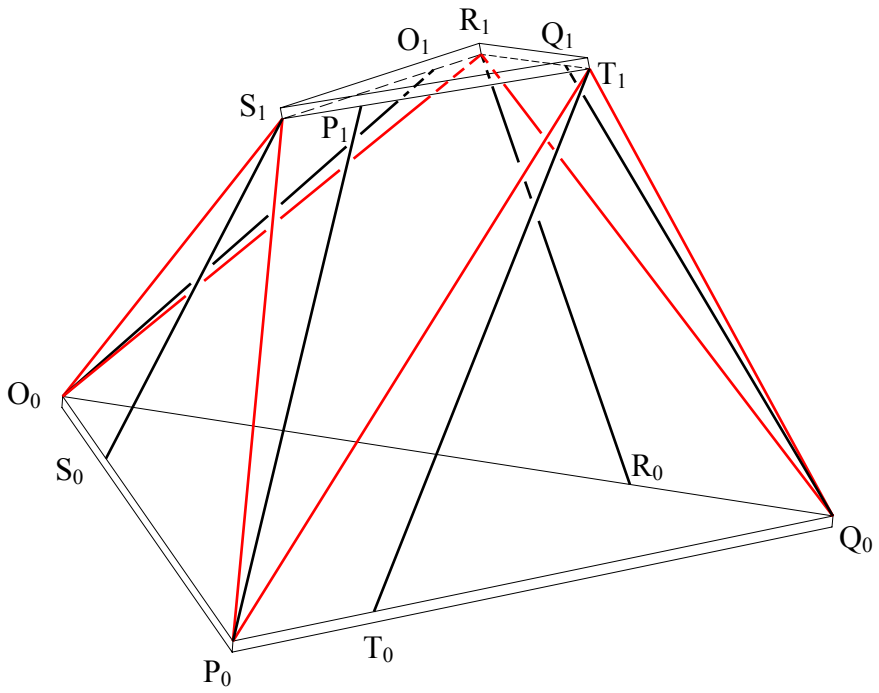

(a)

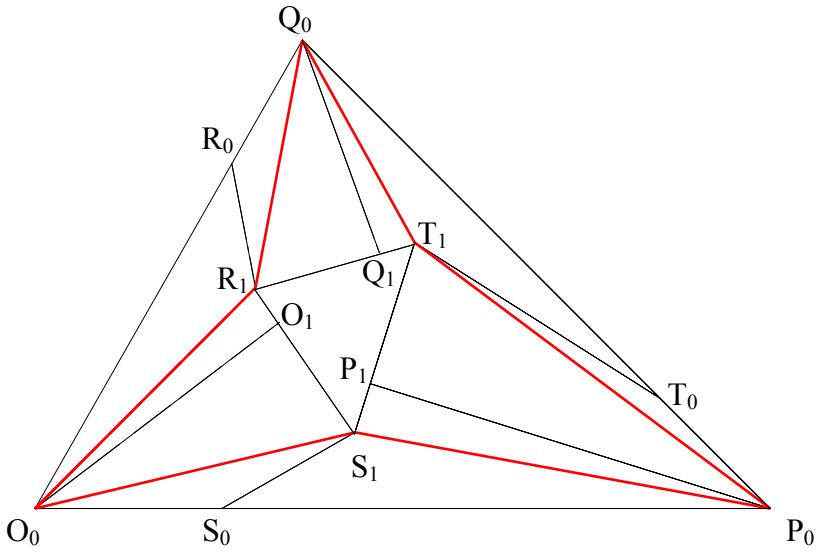

(b)

Figure A1: Special 6-6 Platform and Equivalent 3-3 Platform ;
(a) Perspective View, (b) Plan View

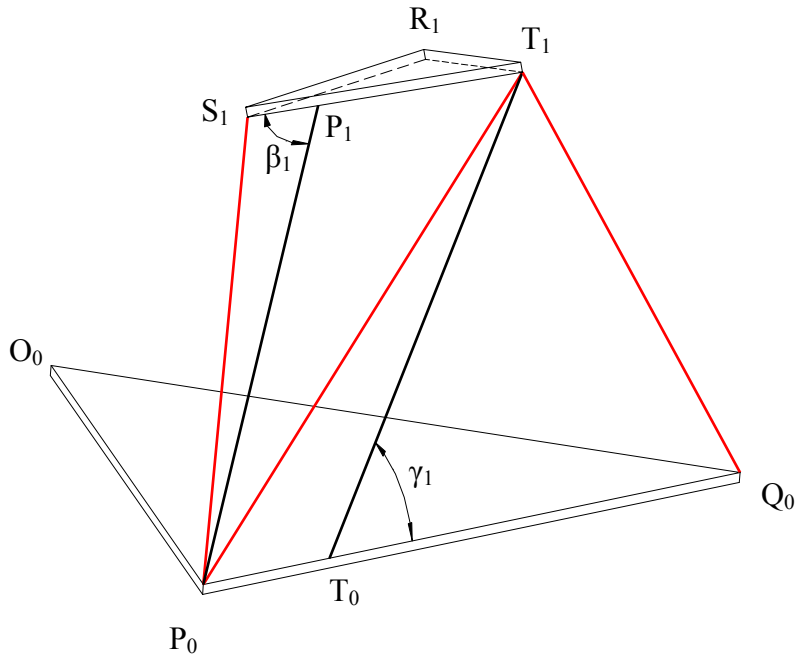

Figure A-2: Definition of Angles β and γ

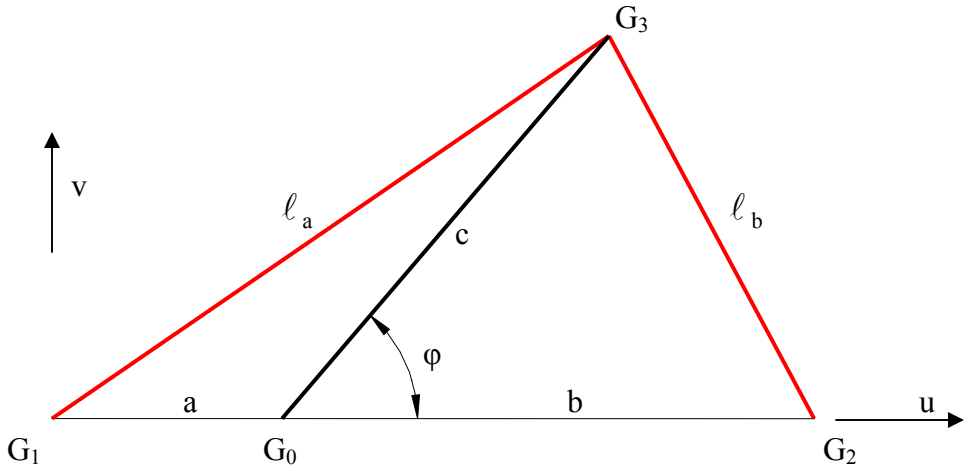

Figure A-3: Planar Triangle

Table 1: Design Objectives

Specification	Range
Individual connector deflection	± 5 mm
Maximum perpendicular load	50 N
Motion range in Z direction	± 4 mm
Motion range in X,Y directions	± 3.5 mm
Rotational range about Z axis	± 6°
Rotational range about X,Y axes	± 4°
Position measurement resolution	0.01 mm

Table 2: Comparison of Magnitudes of Theoretical and Experimental Changes in Wrench

Case	magnitude of $\delta\hat{w}$, N (theoretical)	magnitude of $\delta\hat{w}$, N (experimental)
1	215.1	216.4
2	368.0	370.6
3	114.6	114.7
4	3.014	3.008
5	3.087	2.933
6	12.098	11.335

Table 3: Comparison of Pitches of Theoretical and Experimental Changes in Wrench

Case	pitch of $\delta\hat{w}$, mm (theoretical)	pitch of $\delta\hat{w}$, mm (experimental)
1	0.580	0.672
2	2.311	1.688
3	7.133	7.433
4	-7.386	-7.457
5	-5.729	-6.360
6	3.322	2.863

Table 4: Comparison of Direction and Distance Between the Theoretical and Experimental Changes in Wrench

Case	angle between directions, degrees	perp. distance between lines of action, mm
1	1.816	0.189
2	2.660	0.360
3	1.078	0.004
4	2.187	0.666
5	3.895	1.204
6	9.970	0.453